ACS APPLIED MATERIALS & INTERFACES

Research Article

Cite This: ACS Appl. Mater. Interfaces 2018, 10, 21808−21815

www.acsami.org

Tunable Control of Hydrogel Microstructure by Kinetic Competition between Self-Assembly and Crosslinking of Elastin-like Proteins

Huiyuan Wang,[†] Alexandra Paul,[‡] Duong Nguyen,[‡] Annika Enejder,[†] and Sarah C. Heilshorn*[,†]

[†]Department of Materials Science & Engineering, Stanford University, Stanford, California 94305, United States

[‡]Department of Biology and Biological Engineering, Chalmers University of Technology, Gothenburg SE-412 96, Sweden

Supporting Information

ABSTRACT: The fabrication of three dimensional "bead-string" microstructured hydrogels is rationally achieved by controlling the relative timing of chemical crosslinking and physical self-assembly processes of an engineered protein. To demonstrate this strategy, an elastin-like protein (ELP) amino acid sequence was selected to enable site-specific chemical crosslinking and thermoresponsive physical self-assembly. This method allows the tuning of material microstructures without altering the ELP amino acid sequence but simply through controlling the chemical crosslinking extent before the thermally induced, physical coacervation of ELP. A loosely crosslinked network enables ELP to have greater chain mobility, resulting in phase segregation into larger beads. By contrast, a network with higher crosslinking density has restricted ELP chain mobility, resulting in more localized self-assembly into smaller beads. As a proof of concept application for this facile assembly process, we demonstrate one-pot, simultaneous, dual encapsulation of hydrophilic and hydrophobic model drugs within the microstructured hydrogel and differential release rates of the two drugs from the material.

KEYWORDS: *elastin-like protein (ELP), thermo-responsive, self-assembly, structure, hydrogel*

1. INTRODUCTION

Self-assembly is a ubiquitous process in nature by which a wide variety of complex materials with elaborate structures and unique properties are created.[1,2] Inspired by biological self-assembling systems, many biomimetic molecules and methods have been utilized to facilitate the design and fabrication of three-dimensional (3D) functional materials.[3−5] In particular, peptides and proteins are highly appealing building blocks for constructing self-assembled systems because of their exquisite structures and functions.[6] Elastin-like protein (ELP) is a class of genetically engineered polypeptides with amino acid sequences inspired by tropoelastin, consisting of the pentapeptide repeat Val-Pro-Gly-Xaa-Gly (VPGXG), where the guest residue Xaa can be any amino acid except Pro.[7] ELP can undergo a lower critical solution temperature (LCST) phase transition; that is, it is soluble at temperatures below the transition temperature (T_t) and becomes less soluble and forms polymer-rich coacervates when the temperature is raised above T_t.[8,9] This thermoresponsive assembly behavior of ELP has previously been exploited for diverse applications, including stimuli-responsive drug delivery,[8,10] design of functional materials with highly stretchable and self-adhesive features,[11,12] and modeling the tropoelastin coacervation process in vitro to better understand the elastic fiber assembly.[13,14] Interesting nanofibrous multilayered architectures, string-like networks, and round-shaped protein coacervations were observed previously for materials involving the self-assembly of ELP, and the material structures were found to have a dependence on the primary amino acid sequence of the protein.[11,15] To date, methods that can easily control the self-assembled microstructure of ELP-based materials without requiring redesign of the primary amino acid sequence have not been reported.

Herein, we present an innovative, simple, one-pot method that permits facile fabrication and tuning of 3D "bead-string" microstructures in an ELP hydrogel system without the modification of the amino acid sequence. This is achieved by modulating the timing of the chemical crosslinking and physical self-assembly processes during ELP gelation (Figure 1). By controlling the extent of chemical crosslinking before thermally inducing the physical assembly of ELP, we were able to tune the size and density of polymer-rich coacervates in the material structure. To demonstrate the generalizability of this strategy, we present three different approaches to control the extent of chemical crosslinking: (1) tuning the pH of the gel precursor solution, (2) modifying the stoichiometric ratio of functional groups in the crosslinking reaction, and (3) controlling the crosslinking reaction time before the thermo-triggered assembly. Each of these three methods resulted in the control of the resulting hydrogel microstructure. As a proof of concept, we further demonstrate that the "bead-string" microstructured ELP hydrogel allows simultaneous coencapsulation and sequential release of hydrophilic and hydrophobic drugs in a very simple manner. The delivery of multiple drugs within one hydrogel system[16−18] can be significantly helpful in treating diseases or repairing tissues that involve multiple

Received: February 20, 2018
Accepted: June 5, 2018
Published: June 5, 2018

DOI: 10.1021/acsami.8b02461
ACS Appl. Mater. Interfaces 2018, 10, 21808−21815

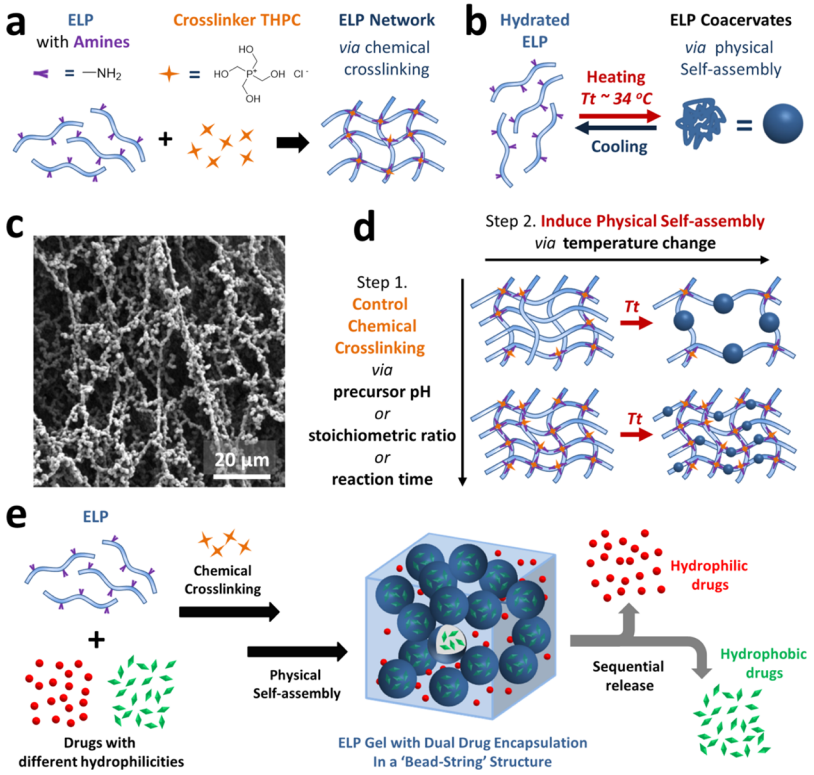

Figure 1. Schematic of ELP hydrogel formation with controlled "bead-string" structure. (a) Covalent crosslinking of ELP network using chemical crosslinker tetrakis(hydroxymethyl)phosphonium chloride (THPC). (b) Thermally triggered physical self-assembly of ELP. (c) SEM image of "bead-string" microstructured ELP gel (5 wt % ELP crosslinked at 1:1 stoichiometric ratio for 2 min at room temperature (RT), followed by 10 min at 37 °C). (d) Proposed strategy to control hydrogel microstructure by modulating chemical crosslinking and physical self-assembly processes of ELP. (e) Simple, one-pot formation of microstructured ELP hydrogel for dual encapsulation and sequential release of hydrophilic and hydrophobic drugs.

complicated signaling pathways.[19−21] However, it is often challenging to achieve codelivery and differential release rates of drugs with different hydrophilicities in one delivery system, which often requires the use of advanced chemistry, sophisticated molecular designs, and multistep fabrication procedures.[22−24] By contrast, here we use a one-pot fabrication method to simultaneously encapsulate the hydrophobic drugs within the hydrophobic, self-assembled ELP coacervates and the hydrophilic drugs within the polymer-lean phase of the gel network. Taken together, we have utilized a facile approach to fabricate hydrogels with unique "bead-string" microstructures, which show the potential for co-delivery and sequential release of drugs with different hydrophilicities (Figure 1).

2. RESULTS AND DISCUSSION

2.1. Formation of ELP Hydrogel with the "Bead-String" Structure. Protein engineering allows molecular-level control over the recombinant protein. Here, we have designed and introduced lysine residues into the ELP sequences to enable site-specific, covalent crosslinking through reaction with the lysine primary amine side chains.[25,26] In this study, we used a previously introduced, amine-reactive crosslinker, THPC, to form ELP hydrogels at RT (Figure 1a).[27] Our ELP will undergo an LCST phase transition, with a characterized T_t of ~33.9 °C (Figure S1, Supporting Information).[28] Therefore, at RT, ELP is fully soluble but will undergo a thermodynamic phase separation to form polymer-rich aggregates distributed within a polymer-lean phase when the temperature is raised to physiological temperature (Figure 1b). This results in a characteristic "bead-string" microstructure, with bead size on the order of 1 μm as observed using scanning electron microscopy (SEM), for an ELP hydrogel that undergoes incomplete THPC crosslinking before heating up to 37 °C (Figure 1c). We hypothesized that the tuning of this microstructure could be achieved by modulating ELP chain mobility via controlling the extent of crosslinking before inducing LCST self-assembly (Figure 1d). We reasoned that in a loosely crosslinked network, the ELP chains would have fewer attachment points to the network and thus greater mobility to phase segregate into larger beads. By contrast, in a network with a higher density of crosslinks, the ELP chains would be more "locked" into place, resulting in more localized self-assembly and smaller beads. We further hypothesized that the extent of crosslinking within the gel could be controlled by several different methods, including tuning the pH of the gel precursor solution, the amount of crosslinker added, or the reaction time at RT before heating above T_t.

2.2. Control of ELP Hydrogel "Bead-String" Structure via pH. To evaluate the hypothesis of controlling the ELP hydrogel microstructure by tuning the crosslinking extent below T_t, we first explored changing the pH of the gel precursor solution. Previous work by Lim et al. reported that the mechanical properties of ELP gels formed via a similar amine-reactive crosslinker were strongly influenced by the reaction pH, with gels showing a higher stiffness at more basic pH.[26] This observation suggests that changes in pH can result in varied ratios of primary amine ($-NH_2$) to protonated amines ($-NH_3^+$) on the ELP chains,[26] thus leading to different

DOI: 10.1021/acsami.8b02461
ACS Appl. Mater. Interfaces 2018, 10, 21808−21815

crosslinking densities. In our study, we tuned the ELP precursor solution to have a pH of 6.5, 7.5, or 8.5, before crosslinking. We observed a similar trend in the effect of pH on hydrogel mechanics as previously reported; gels crosslinked at pH 8.5 reached a plateau G' of ∼800 Pa, whereas gels crosslinked at pH 6.5 resulted in a G' of ∼10 Pa (Figure 2a). In addition, the gelation time was significantly affected by the pH of the ELP precursor solution. Nearly complete gelation occurred in approximately 1, 7, or 40 min for reactions with pH of 8.5, 7.5, or 6.5, respectively (Figure 2a). Therefore, a crosslinking time period of 15 min was selected to enable the formation of networks at RT with three different crosslinking extents: highly crosslinked at pH 8.5, intermediate at 7.5, and barely crosslinked at 6.5. Following this, a 15 min incubation at 37 °C was applied to induce the thermal phase separation of ELP.

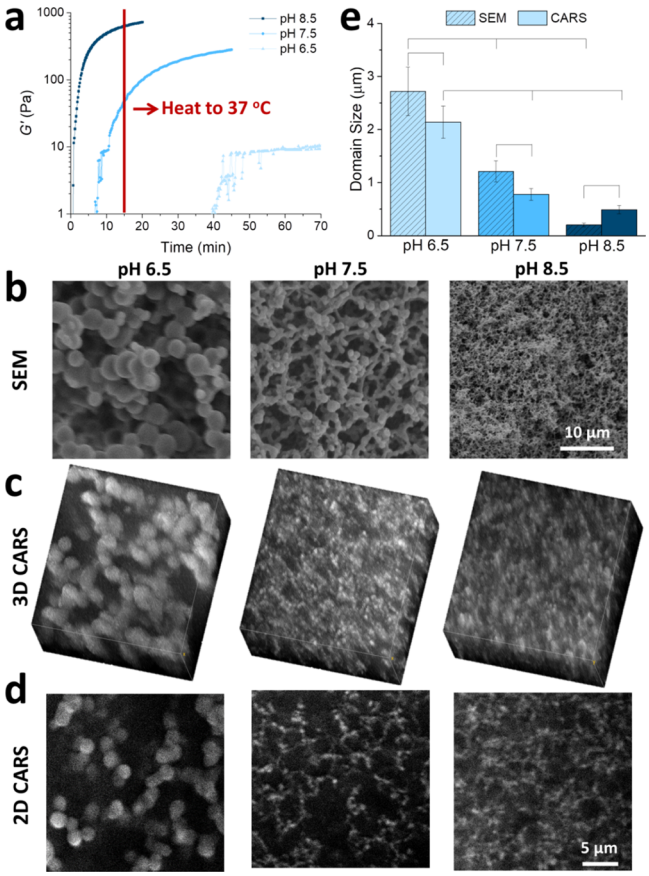

Figure 2. Control of ELP hydrogel microstructure via pH of precursor solution. (a) Oscillatory time sweep rheology of 5 wt % ELP at 1:1 crosslinking ratio with varied pH at 25 °C without thermally induced physical self-assembly. Vertical line represents the selected reaction time used to prepare ELP networks with different crosslinking extents before thermal heating above T_t. (b) SEM images of ELP hydrogels formed at different pH. (c) 3D reconstruction of CARS images of ELP hydrogels formed at different pH. (d) Selected single z-slice CARS images of ELP hydrogels formed at different pH. (e) Quantification results of "bead" size in different ELP hydrogels.

Consistent with our hypothesis (Figure 1d), we found that gels starting from a barely crosslinked network before heating above T_t were characterized as having larger self-assembled aggregates, ∼2.7 μm, whereas gels formed from highly crosslinked ELP had a microstructure with a dense network of smaller beads, ∼0.2 μm (Figure 2b). Notably, a critical point drying (CPD) method was selected to prepare SEM samples for gel microstructure characterization instead of the commonly used freeze-drying method.[29−31] Previous studies have shown that biological samples prepared using freeze-drying and CPD methods can exhibit different structures during SEM characterization, and freeze-drying was found to cause more structural artifacts and damage compared with CPD.[32,33] To investigate if different sample drying methods can result in varied ELP hydrogel microstructure, we prepared two hydrogels using the same formulation and fabrication procedure but dried through freeze drying or CPD. SEM results demonstrated that the distinct bead-string structure of our ELP hydrogel can only be observed in the sample dried by CPD. In the freeze-dried samples, the beads appeared to have merged together into larger structures (Figure S2, Supporting Information). This is likely due to the fact that the temperature used in the freeze-drying method is much lower than the T_t of our ELP (33.9 °C), thus leading to an inability to maintain the thermally induced, self-assembled aggregates during the lyophilization process.

Although samples prepared using the CPD method appeared to offer better structural details than the freeze-drying method, the potential concern of specimen structural change associated with CPD sample preparation still exists.[34] To completely bypass the need for sample dehydration, we used an alternative imaging modality, coherent anti-Stokes Raman scattering (CARS) microscopy, to observe the structure of our ELP hydrogels at 37 °C in its native, hydrated state (Figure 2c,d). Similar to the structures observed in samples prepared by CPD and imaged with SEM, a bead-string structure was observed by CARS in our ELP hydrogels. These samples also confirmed the previously observed trend, with barely crosslinked networks at a lower pH forming larger beads after heating above T_t, while gels prepared at higher pH forming denser structures with smaller beads (Figures 2d,e and S3, Supporting Information). Compared with data acquired by SEM, the bead size observed in the CARS images was slightly smaller at both pH 6.5 and pH 7.5 (Figure 2e). This may be because of the use of ethanol in the CPD process for SEM sample preparation, as previous studies showed that elastin swells in ethanol.[35,36] Under the condition of pH 8.5, however, a domain quantification of CARS images showed slightly larger sizes (Figure 2e). The reason for this may be that the size of the thermal domains in these samples was below the resolution limit of CARS, approximately 350 nm laterally.[37]

2.3. Control of the ELP Hydrogel Structure via the Stoichiometric Ratio or Reaction Time. To further prove our hypothesis of controlling the hydrogel microstructure by varying the extent of chemical crosslinking before inducing physical self-assembly, we next evaluated an alternative approach to tune crosslinking density by varying the stoichiometric ratio of the functional groups involved in the crosslinking reaction.[38] In our study, we achieved this by keeping the ELP concentration constant but varying the concentration of the THPC crosslinker to control the stoichiometric ratio of hydroxyls (on THPC) to amines (on ELP). For stoichiometric ratios of 0.3, 0.5, and 1.0, the corresponding plateau moduli G' were ∼50, 160, and 890 Pa, respectively (Figure 3a). This is consistent with previous findings that higher stoichiometric ratios result in higher crosslinking densities and hence in higher gel stiffness.[39,40] A reaction time point of 45 min at RT was selected to ensure full

DOI: 10.1021/acsami.8b02461
ACS Appl. Mater. Interfaces 2018, 10, 21808−21815

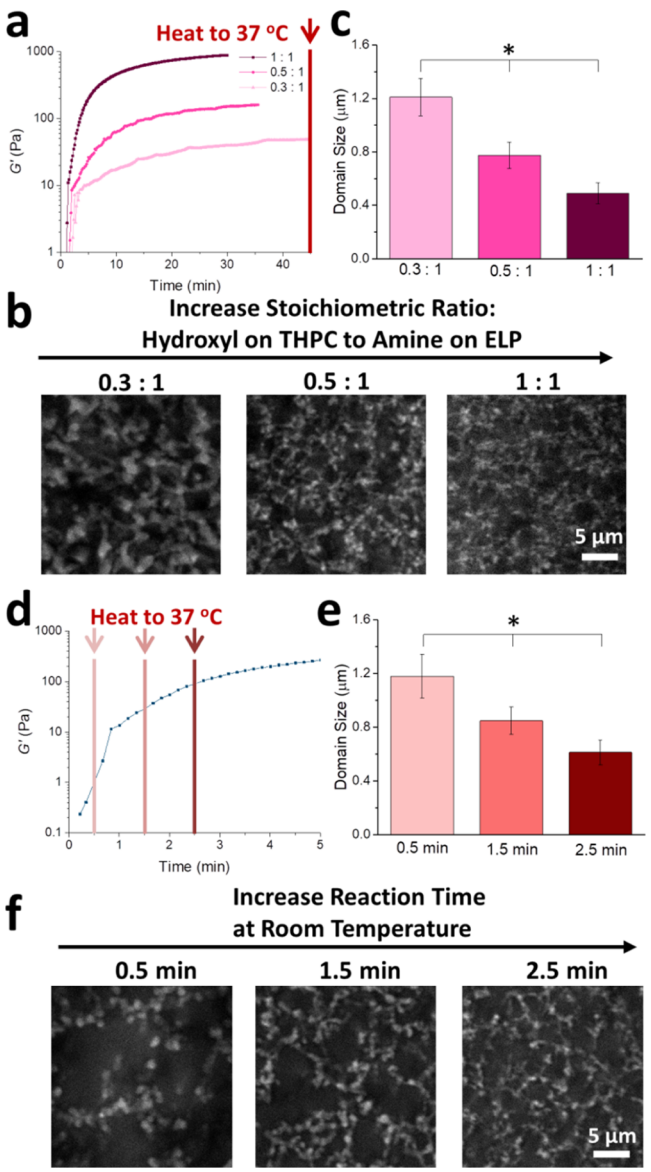

Figure 3. Control of ELP hydrogel microstructure via stoichiometric ratio (a–c) or chemical reaction time (d–f). (a) Oscillatory time sweep rheology of 5 wt % ELP formed with different crosslinking stoichiometric ratios at 25 °C. Vertical line represents the selected reaction time used to prepare ELP networks with different crosslinking extents before thermal heating above T_t. (b) Selected single z-slice CARS images of ELP hydrogels formed at different stoichiometric ratios. (c) Quantification results of "bead" size in different ELP hydrogels. (d) Oscillatory time sweep rheology of 5 wt % ELP formed with precursor pH of 8.5 and 1:1 stoichiometric ratio at 25 °C. (e) Selected single z-slice CARS images of ELP hydrogels formed with different chemical reaction times. (f) Quantification results of "bead" size in different ELP hydrogels.

gelation for all three stoichiometric ratio conditions (Figure 3a), followed by a 15 min incubation at 37 °C to induce self-assembly of ELP thermal aggregates. Observations of the hydrogel structures using CARS microscopy revealed that the gel formed with the lowest stoichiometric ratio had the largest self-assembled domains, ~1.2 μm, while the smallest beads, ~0.5 μm, were observed in the gel with the highest crosslinking density (Figure 3b,c).

As a third demonstration, we next controlled the extent of chemical crosslinking by varying the reaction time while keeping the pH and stoichiometric ratio constant.[41] The chemical crosslinking reaction was allowed to proceed at RT for 0.5, 1.5, or 2.5 min before transferring the samples to 37 °C to induce physical self-assembly (Figure 3d). Again, gel structures were observed while fully hydrated using CARS microscopy. Gels induced to self-assemble after the shortest chemical reaction time, when the network crosslinking density was still low, had the largest domain sizes, ~1.2 μm (Figure 3e,f). By contrast, longer chemical reaction times resulted in a higher crosslinking extent and smaller aggregates (Figure 3e,f). Thus, all three experimental strategies resulted in a similar trend, with greater network crosslinking leading to smaller bead microstructures. These data are consistent with our hypothesis that covalent crosslinks will limit the mobility of the ELP chains during physical self-assembly and thus provide a facile method to tune gel microstructure.

2.4. Controlled Distribution of a Model Drug in Microstructured ELP. The ELP materials used in this study have been shown to be biocompatible in previous biomedical applications.[27,28,40] To explore the possibility of using our microstructured ELP hydrogel for drug delivery, we encapsulated gold nanoparticles (Au NPs) in the gels. Gold NPs show great promise for applications in drug and gene delivery,[42−44] and enable easy visualization of their distribution in the hydrogel based on their strong, multiphoton excited photoluminescence without attaching artificial labeling molecules.[45] This allowed us to evaluate simultaneously the protein-rich microdomains using the CARS signal, with the distribution of the Au NPs using multiphoton-excited photoluminescence. We hypothesized that the known hydrophobic nature of Au NPs would enable their selective encapsulation within the ELP-rich beads. Experimental results from multiple hydrogel formation procedures confirmed the formation of "bead-string" structured ELP hydrogels in the presence of Au NPs, and the Au NPs were localized within the protein-rich domains (Figure 4a,b), presumably because of hydrophobic and ionic interactions between the Au NPs and proteins.[46,47] Consistent with our observations in the absence of Au NPs, bead size was controlled by tuning of pH or reaction time. The sizes of the domains were quantified to be slightly smaller than those without Au NPs, though within the variability observed for different gel preparations (Figure 4c).

2.5. Dual Encapsulation and Sequential Release of Hydrophilic and Hydrophobic Drugs. Encouraged by the selective distribution of the Au NPs within the hydrophobic, self-assembled domains embedded in a hydrated matrix of ELP (Figure 4), we hypothesized that it would be possible to achieve dual encapsulation of hydrophilic and hydrophobic therapeutics in these materials. We further hypothesized that drugs with different hydrophilicities would spontaneously partition into the ELP-rich (hydrophobic molecules) and ELP-lean (hydrophilic molecules) structures within the gel network, ultimately resulting in different release kinetics. To verify these hypotheses, we simultaneously encapsulated coumarin-6 as a model hydrophobic drug[48] and rhodamine B isothiocyanate–dextran as a model hydrophilic drug and monitored their distribution within the microstructured ELP hydrogels using confocal microscopy. Interestingly, after the formation of the gel–drug construct, the hydrophobic drug was found to be localized in the thermal aggregates, whereas the hydrophilic drug was found to predominantly disperse in the polymer-lean phase of the hydrogel (Figure 5a,b). As expected, the quantification of the release profiles revealed that

DOI: 10.1021/acsami.8b02461
ACS Appl. Mater. Interfaces 2018, 10, 21808–21815

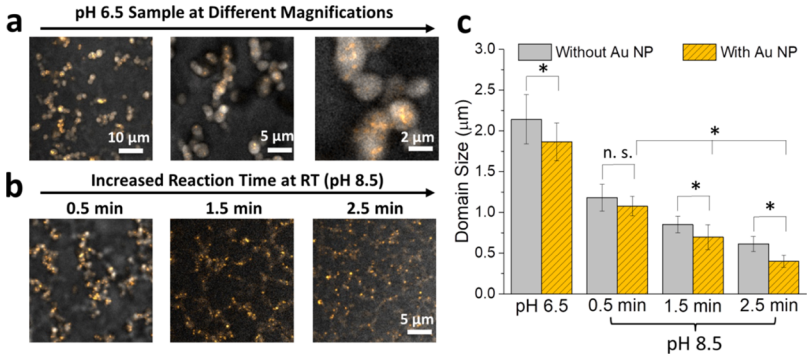

Figure 4. Encapsulation of Au nanoparticles (Au NPs) in ELP hydrogels. (a) CARS images of Au NPs encapsulated within ELP gels, formed at pH 6.5 and observed using different magnifications. The Au NPs provide exceptional contrast and appear as bright spots within the self-assembled domains (gray region). (b) CARS images of Au NPs encapsulated within ELP gels, formed at pH 8.5 with varied reaction time at RT. (c) Quantification of protein-rich domain sizes for different ELP gels with or without Au NPs.

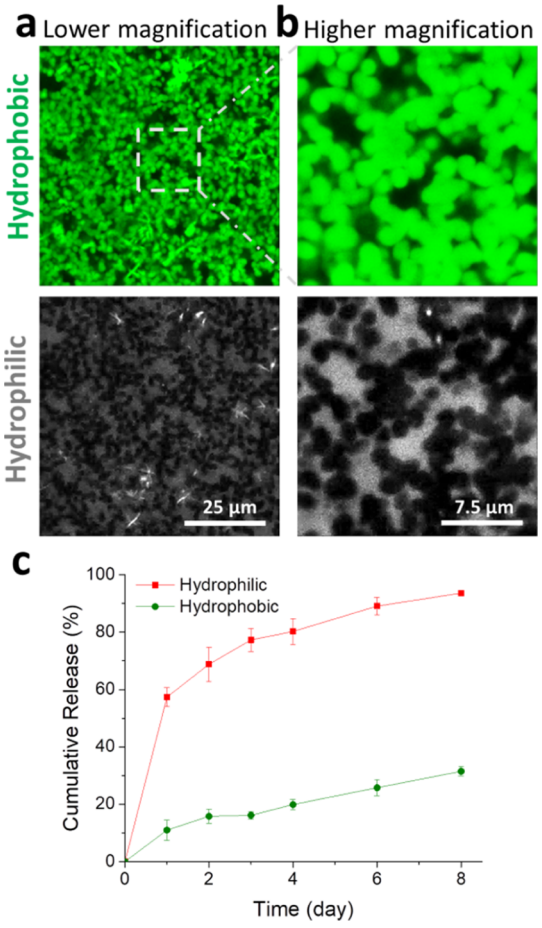

Figure 5. Simultaneous encapsulation and sequential release of hydrophilic and hydrophobic drugs in ELP hydrogels. (a,b) Confocal images demonstrating spontaneous spatially controlled distribution of a hydrophobic model drug, coumarin-6 (green), and a hydrophilic model drug, dextran (gray), within a microstructured ELP hydrogel before drug release at lower (a) and higher (b) magnification. (c) Cumulative release of hydrophobic and hydrophilic drugs from ELP gels.

the encapsulated hydrophilic drugs have a faster release rate compared with the hydrophobic drugs (Figure 5c). This is presumably because of the much larger polymer network mesh size found in the polymer-lean phase where the hydrophilic drug is located, while the polymer-rich phase where the hydrophobic drug is located has a much smaller mesh size because of the relatively high polymer content. Thus, a novel one-pot method was identified to enable the simultaneous encapsulation and sequential release of two different drugs with different hydrophilicities, which is an ongoing challenge in drug delivery and is likely to become an increasingly employed strategy for new therapies.[22,24,49] We further studied the influence of microstructure on gel stability and drug release profiles. Experimental results showed that gels formed at pH 7.5 with the intermediate mechanical strength (Figure 2a) and "bead-string" network structure (Figure 2b–d) had the highest gel stability compared with gels formed at pH of 6.5 and 8.5 (Figure S4, Supporting Information). This is likely because of a trade-off between the effects of enhanced mechanical strength and an increase in the microscale surface area that is susceptible to erosion. As expected, co-encapsulated hydrophilic and hydrophobic drugs were found to be released from the hydrogels at different rates, with over 80% of the hydrophilic drug released in 4 days (Figure S5, Supporting Information) while only 13–25% of the hydrophobic drug was released at this same time point (Figure S6, Supporting Information). No significant differences in release rates for hydrophilic drugs from the ELP gels with different microstructures were observed (Figure S5, Supporting Information). This is to be expected, as the hydrophilic drug is encapsulated within the polymer-lean portion of the ELP hydrogel, which does not present a significant barrier to passive diffusion. By contrast, the hydrophobic drug had the slowest release rate from the ELP hydrogel with the intermediate "bead-string" network structure (Figure S6, Supporting Information). Interestingly, this was also the network structure with the slowest gel erosion rate (Figure S4, Supporting Information), suggesting that the hydrophobic drugs are mainly encapsulated inside of the polymer-rich ELP thermal aggregates and are primarily released because of gel erosion.

3. CONCLUSIONS

We have reported a unique physicochemical method to rationally control the bead-string microstructure within a self-assembled, protein-engineered hydrogel without altering the primary amino acid sequence. This is achieved by controlling the timing of the chemical crosslinking process relative to the physical self-assembly process. Specifically, we modify the extent of chemical crosslinking that occurs before inducing the thermal phase transition. Three different

DOI: 10.1021/acsami.8b02461
ACS Appl. Mater. Interfaces 2018, 10, 21808–21815

experimental strategies were used to achieve this control, and in each case, a greater extent of chemical crosslinking resulted in smaller structural features. Proof-of-concept experiments demonstrated that the resulting bead-string microstructure could be exploited for dual encapsulation of hydrophilic and hydrophobic drugs, with the hydrophilic drugs spontaneously distributing within the polymer-lean phase of the hydrogel and hydrophobic drugs preferentially locating within the self-assembled, polymer-rich domains. This interesting distribution phenomenon resulted in differential release rates for the encapsulated drugs. Taken together, these data demonstrate a novel strategy to rationally control the size of a self-assembled, bead-string microstructure. Importantly, this control was exerted during the fabrication stage using the same engineered protein throughout all studies, without any modification to the underlying amino acid sequence. These materials may be useful for a range of applications where microstructure control is desired, including drug delivery.

4. EXPERIMENTAL METHODS

4.1. ELP Expression and Purification. The design and synthesis of a modular recombinant ELP, containing lysine residues to act as amine-reactive crosslinking sites, were previously reported.[50,51] The amino acid sequence of ELP used in this study, MASMTGGQQMG–HHHHH–DDDDK–TVYAVTGRGDSPASSAA–$[(VPGIG)_2$ VPGKG $(VPGIG)_2]_3$VP, was previously reported.[51] ELP was expressed and purified using the standard recombinant protein technology. Briefly, protein sequences were cloned into pET15b plasmids; expressed in *Escherichia coli*, strain BL21 (DE3); and induced with 1 mM isopropyl β-D-1-thiogalactopyranoside (IPTG) at an OD600 of 0.8 for 6 h. The harvested cell pellets were suspended and lysed by three freeze–thaw cycles, as previously reported.[51] The lysates were then adjusted to pH of 3, 6, or 9 with hydrochloric acid (HCl) and/or sodium hydroxide (NaOH) before being purified by iterative inverse temperature-cycling. Protein molecular weight and purity were confirmed by sodium dodecyl sulfate polyacrylamide gel electrophoresis. Purified ELP was dialyzed three times (10 000 MWCO, 36 h, 4 °C, deionized water) to desalt. The ELP was then lyophilized and stored at 4 °C until use.

4.2. Formation of ELP Hydrogels. Lyophilized ELP was solubilized in chilled phosphate buffered saline (PBS) (1×, pH 7.4) at a stock concentration of 6.25 wt % and dissolved by vortex. ELP purified at pH 3, 6, or 9 resulted in a stock solution with pH 6.5, 7.5, or 8.5, respectively. Air bubbles were removed by centrifugation, and the final solutions were kept on ice until use. An initial crosslinker stock solution of THPC (Sigma-Aldrich) was prepared in PBS and kept on ice. The stoichiometric crosslinking ratio (X) of crosslinker reactive hydroxyl groups (4 per THPC molecule) to total primary amine groups (14 per ELP chain) was varied by adjusting the concentration of THPC stock solution during the experiments. The hydrogel precursor solutions were mixed with the crosslinker at a 4:1 volume ratio to yield crosslinked hydrogels that consisted of 5 wt % ELP. Crosslinking ratios of 0.3, 0.5, and 1 were used in different experiments. Reaction time at RT was varied from 0.5, 1.5, 2.5, 15, or 45 min before incubating the gel at 37 °C to induce self-assembly. After incubation at 37 °C for 15 min, the gels were submerged with PBS to keep them hydrated.

4.3. Preparation of Au NPs. Gold NPs (sized 50 nm) were prepared from $HAuCl_4$ in water/citrate media using the Turkevich method.[52] The nanoparticles were functionalized with polyvinylpyrrolidone (PVP) over 24 h and then purified by means of centrifugation and redispersed in Milli-Q water. The final concentration of gold in the preparations was 0.08 mg/mL, and the particle concentration was approximately 7.91×10^{10} particles/mL. To encapsulate the Au NPs in ELP gels, the solution of Au NPs was first well mixed with the stock ELP solution, followed by the addition of crosslinker THPC to form a hydrogel, as the methods describe in the previous section.

4.4. Hydrogel Mechanical Characterization. Mechanical testing was performed on a stress-controlled rheometer (ARG2, TA Instruments) using a 20 mm diameter, cone-on-plate geometry. Samples were allowed to gel in situ on the rheometer, and a humidity chamber was secured in place to prevent dehydration. To evaluate the gelation kinetics for different formulations, time sweeps were performed at an oscillatory stress of 4.74 Pa at 25 °C.

4.5. Characterization with SEM. ELP hydrogels were prepared using the methods described in the previous section and equilibrated at 37 °C overnight before sample drying. Two sample preparation procedures were compared. For the freeze-drying method, ELP hydrogels were frozen at −80 °C overnight and then dried in a lyophilizer. For the CPD method, hydrogels were sequentially dehydrated in 30, 50, 70, 90, and 100% ethanol for 10 min each, followed by another 10 min in 100% ethanol before CPD with tousimis Autosamdri-815. A 10 nm Au/Pd coating was then applied using a Denton Vacuum Desk II and DTM-100 thickness monitor system before imaging with a Hitachi S-3400N variable pressure scanning electron microscope.

4.6. Characterization with CARS Microscopy. The ELP aggregate formation was assessed in situ using CARS microscopy by tuning to the carbon–hydrogen CH_3 stretching vibration at 2930 cm^{-1},[53] characteristic for proteins. The vibration was driven by overlapping two ps-pulsed laser beams at wavelengths 1064 and 811 nm, respectively, in time and space in the focal plane of an inverted microscope (Eclipse TE2000-E with a C1 confocal microscope scanning head, Nikon; objective: Nikon Plan Fluor, 40×, NA 1.30). The laser beams were generated by a laser system consisting of a Nd/vanadate laser (1064 and 532 nm, 7 ps, 76 MHz, PicoTRAIN, HighQ Lasers GmbH, Hohenems, Austria) and an optical parametric oscillator (tuned to 811 nm, Levante Emerald OPO, Angewandte Physik & Elektronik GmbH, Berlin, Germany, tunable between 690 and 900 nm). The deep penetration of the near-infrared excitation beams enables the characterization of hydrated ELP scaffolds without concern for potential edge effects. Furthermore, because CARS microscopy does not require the use of labels, concerns over label photodegradation, limited 3D diffusion of labeling molecules, or disruption of the true ELP microstructure because of the presence of labels were avoided. The emission of the CARS signal is limited to the high-intensity region of the focal volume, enabling a spatial resolution of 350 nm in the xy plane. The two excitation beams were simultaneously scanned over the sample, and the CARS signal was detected in transmission mode with a single-photon counting detector (Becker & Hickl GmbH). By means of a second detection channel, the back reflected multiphoton excited photoluminescence from Au NPs could simultaneously be recorded between 490 and 540 nm. Dichroic mirrors and high-optical-density filters were used to separate the CARS and photoluminescence signals, respectively, as well as from the excitation beams before the detector. For detailed information on the experimental setup used for CARS microscopy, the interested reader is referred to the previously published work.[54]

4.7. Hydrophobic and Hydrophilic Drug Distribution and Release Study. Hydrophilic rhodamine B isothiocyanate–dextran (70 kDa, Sigma-Aldrich) and hydrophobic coumarin-6 (Sigma-Aldrich) were selected as the model drugs for in vitro drug encapsulation and release studies. Coumarin-6 is a fluorescent molecule with very low solubility in water and has been used frequently as a model hydrophobic drug to evaluate drug delivery systems in vitro and in vivo.[48] Stock solutions of dextran and coumarin-6 were prepared by dissolving the two model drugs in PBS and dimethylformamide (DMF), respectively. Dextran and coumarin-6 were mixed with ELP solution in PBS first and immediately pulsed with a vortex for 2–4 s to facilitate the dispersal of hydrophobic model drug in the aqueous solution. THPC crosslinker was added next, followed by another vortex step to prevent the sedimentation of the hydrophobic model drug and to enhance homogeneous encapsulation throughout the ELP gel at a final ELP concentration of 5 wt %, dextran concentration of 0.5 mg/mL, and coumarin-6

DOI: 10.1021/acsami.8b02461
ACS Appl. Mater. Interfaces 2018, 10, 21808–21815

concentration of 0.25 mM. The gel was prepared at pH 6.5, 1:1 stoichiometric ratio, 15 min at RT followed by 15 min at 37 °C. A Gel−drug construct (50 μL) was made in a 1.5 mL Eppendorf centrifuge tube and immersed in 1 mL PBS. The samples were incubated at 37 °C in the orbital shaker at a speed of 50 rpm. At predetermined time points (every 24 h for the first 4 days and every 48 h after that until day 8), 200 μL of the solution was collected and replaced by fresh PBS. The release of model drugs was monitored by measuring the fluorescence intensity (dextran: λ_{exc} 543 nm, λ_{em} 580 nm; coumarin-6: λ_{exc} 458 nm, λ_{em} 510 nm) of the collected solution using a SpectraMax M2 microplate reader. The distribution of the model drugs within the gels was visualized at 37 °C using a Leica SPE confocal microscope.

4.8. Characterization of Hydrogel Mass Loss. ELP hydrogels were prepared using the methods described above with a gel volume of 50 μL in a 1.5 mL Eppendorf centrifuge tube. The hydrogel samples were immersed in 1 mL PBS (1×, pH 7.4, Sigma-Aldrich) and incubated at 37 °C in the orbital shaker at a speed of 50 rpm. At predetermined time points, the remaining mass of the hydrogel was measured after carefully removing and blotting off excess liquid. After each measurement, 1 mL fresh PBS was added to each sample tube. The percentage of remaining hydrogel mass was calculated as (remaining mass after incubation)/(initial mass) × 100%. All measurements were performed in triplicate.

4.9. Statistical Analysis. All data (domain size and cumulative drug release) are represented as mean ± standard deviation (N = 30 for domain size analysis, N = 3 for drug release). The statistical difference between samples was analyzed by one-way ANOVA. For all statistical tests, a threshold value of α = 0.05 was chosen, and a p-value at or below 0.05 indicated significance.

■ ASSOCIATED CONTENT

Supporting Information

The Supporting Information is available free of charge on the ACS Publications website at DOI: 10.1021/acsami.8b02461.

Transmittance (λ = 500 nm) versus temperature for ELP; SEM images of ELP hydrogels prepared with freeze-drying method or CPD method; CARS images of the "bead-string" structure within ELP hydrogels; hydrogel erosion profiles for ELP hydrogels (5 wt %) formed at pH of 6.5, 7.5, and 8.5; cumulative release of hydrophilic drugs from ELP hydrogels (5 wt %) formed at pH of 6.5, 7.5, and 8.5; cumulative release of hydrophobic drugs from ELP hydrogel (5 wt %) formed at pH of 6.5, 7.5, and 8.5 (PDF)

■ AUTHOR INFORMATION

Corresponding Author

*E-mail: heilshorn@stanford.edu.

ORCID

Alexandra Paul: 0000-0002-8368-9880

Sarah C. Heilshorn: 0000-0002-9801-6304

Funding

The authors acknowledge funding provided by NSF DMR-1508006, NIH R21-HL-138042, NIH R21-EB-018407, NIH U19-AI-116484, and California Institute for Regenerative Medicine RT3-07948 (S.C.H.), Kodak Fellowship (H.W.), EU FP7 Marie Curie Innovative Training Network Grant 607842 (A.P. and A.E.), and the Olle Engkvist Foundation (A.E.).

Notes

The authors declare no competing financial interest.

■ ACKNOWLEDGMENTS

The authors acknowledge Dr. Cindy Chung and Dr. Rebecca DiMarco for their thoughtful discussions in ELP hydrogel formation and structure characterization. The Au NPs were kindly prepared by Dr. Daniele Franchi, Department of Chemistry "U. Schiff", University of Florence.

■ REFERENCES

(1) Whitesides, G. M.; Grzybowski, B. Self-Assembly at All Scales. *Science* **2002**, *295*, 2418−2421.

(2) Mendes, A. C.; Baran, E. T.; Reis, R. L.; Azevedo, H. S. Self-Assembly in Nature: Using the Principles of Nature to Create Complex Nanobiomaterials. *Wiley Interdiscip. Rev.: Nanomed. Nanobiotechnol.* **2013**, *5*, 582−612.

(3) Zhang, S. Fabrication of Novel Biomaterials through Molecular Self-Assembly. *Nat. Biotechnol.* **2003**, *21*, 1171−1178.

(4) Hartgerink, J. D.; Beniash, E.; Stupp, S. I. Self-Assembly and Mineralization of Peptide-Amphiphile Nanofibers. *Science* **2001**, *294*, 1684−1688.

(5) Huebsch, N.; Mooney, D. J. Inspiration and Application in the Evolution of Biomaterials. *Nature* **2009**, *462*, 426−432.

(6) Rajagopal, K.; Schneider, J. P. Self-Assembling Peptides and Proteins for Nanotechnological Applications. *Curr. Opin. Struct. Biol.* **2004**, *14*, 480−486.

(7) Betre, H.; Setton, L. A.; Meyer, D. E.; Chilkoti, A. Characterization of a Genetically Engineered Elastin-like Polypeptide for Cartilaginous Tissue Repair. *Biomacromolecules* **2002**, *3*, 910−916.

(8) Chilkoti, A.; Dreher, M. R.; Meyer, D. E.; Raucher, D. Targeted Drug Delivery by Thermally Responsive Polymers. *Adv. Drug Deliv. Rev.* **2002**, *54*, 613−630.

(9) Dreher, M. R.; Simnick, A. J.; Fischer, K.; Smith, R. J.; Patel, A.; Schmidt, M.; Chilkoti, A. Temperature Triggered Self-Assembly of Polypeptides into Multivalent Spherical Micelles. *J. Am. Chem. Soc.* **2008**, *130*, 687−694.

(10) Ryu, J. S.; Raucher, D. Elastin-like Polypeptide for Improved Drug Delivery for Anticancer Therapy: Preclinical Studies and Future Applications. *Expet Opin. Drug Deliv.* **2015**, *12*, 653−667.

(11) Inostroza-Brito, K. E.; Collin, E.; Siton-Mendelson, O.; Smith, K. H.; Monge-Marcet, A.; Ferreira, D. S.; Rodríguez, R. P.; Alonso, M.; Rodríguez-Cabello, J. C.; Reis, R. L.; et al. Co-Assembly, Spatiotemporal Control and Morphogenesis of a Hybrid Protein-Peptide System. *Nat. Chem.* **2015**, *7*, 897−904.

(12) Gonzalez, M. A.; Simon, J. R.; Ghoorchian, A.; Scholl, Z.; Lin, S.; Rubinstein, M.; Marszalek, P.; Chilkoti, A.; López, G. P.; Zhao, X. Strong, Tough, Stretchable, and Self-Adhesive Hydrogels from Intrinsically Unstructured Proteins. *Adv. Mater.* **2017**, *29*, 1604743.

(13) Yeo, G. C.; Keeley, F. W.; Weiss, A. S. Coacervation of Tropoelastin. *Adv. Colloid Interface Sci.* **2011**, *167*, 94−103.

(14) Cirulis, J. T.; Keeley, F. W. Kinetics and Morphology of Self-Assembly of an Elastin-like Polypeptide Based on the Alternating Domain Arrangement of Human Tropoelastin. *Biochemistry* **2010**, *49*, 5726−5733.

(15) Muiznieks, L. D.; Keeley, F. W. Proline Periodicity Modulates the Self-Assembly Properties of Elastin-like Polypeptides. *J. Biol. Chem.* **2010**, *285*, 39779−39789.

(16) Perale, G.; Rossi, F.; Santoro, M.; Peviani, M.; Papa, S.; Llupi, D.; Torriani, P.; Micotti, E.; Previdi, S.; Cervo, L.; et al. Multiple Drug Delivery Hydrogel System for Spinal Cord Injury Repair Strategies. *J. Controlled Release* **2012**, *159*, 271−280.

(17) Battig, M. R.; Soontornworajit, B.; Wang, Y. Programmable Release of Multiple Protein Drugs from Aptamer-Functionalized Hydrogels via Nucleic Acid Hybridization. *J. Am. Chem. Soc.* **2012**, *134*, 12410−12413.

(18) Azagarsamy, M. A.; Anseth, K. S. Wavelength-Controlled Photocleavage for the Orthogonal and Sequential Release of Multiple Proteins. *Angew. Chem., Int. Ed.* **2013**, *52*, 13803−13807.

(19) Simmons, C. A.; Alsberg, E.; Hsiong, S.; Kim, W. J.; Mooney, D. J. Dual Growth Factor Delivery and Controlled Scaffold

DOI: 10.1021/acsami.8b02461
ACS Appl. Mater. Interfaces 2018, 10, 21808−21815

Degradation Enhance in Vivo Bone Formation by Transplanted Bone Marrow Stromal Cells. *Bone* **2004**, *35*, 562−569.
(20) Holland, T. A.; Tabata, Y.; Mikos, A. G. Dual Growth Factor Delivery from Degradable Oligo(poly(ethylene Glycol) Fumarate) Hydrogel Scaffolds for Cartilage Tissue Engineering. *J. Controlled Release* **2005**, *101*, 111−125.
(21) Sun, G.; Shen, Y.-I.; Kusuma, S.; Fox-Talbot, K.; Steenbergen, C. J.; Gerecht, S. Functional Neovascularization of Biodegradable Dextran Hydrogels with Multiple Angiogenic Growth Factors. *Biomaterials* **2011**, *32*, 95−106.
(22) Park, J.; Wrzesinski, S. H.; Stern, E.; Look, M.; Criscione, J.; Ragheb, R.; Jay, S. M.; Demento, S. L.; Agawu, A.; Licona Limon, P.; et al. Combination delivery of TGF-β inhibitor and IL-2 by nanoscale liposomal polymeric gels enhances tumour immunotherapy. *Nat. Mater.* **2012**, *11*, 895−905.
(23) Liu, Y.; Fang, J.; Kim, Y.-J.; Wong, M. K.; Wang, P. Codelivery of Doxorubicin and Paclitaxel by Cross-Linked Multilamellar Liposome Enables Synergistic Antitumor Activity. *Mol. Pharm.* **2014**, *11*, 1651−1661.
(24) Appel, E. A.; Tibbitt, M. W.; Webber, M. J.; Mattix, B. A.; Veiseh, O.; Langer, R. Self-Assembled Hydrogels Utilizing Polymer-Nanoparticle Interactions. *Nat. Commun.* **2015**, *6*, 6295.
(25) Heilshorn, S.; DiZio, K. A.; Welsh, E. R.; Tirrell, D. A. Endothelial Cell Adhesion to the Fibronectin CS5 Domain in Artificial Extracellular Matrix Proteins. *Biomaterials* **2003**, *24*, 4245−4252.
(26) Lim, D. W.; Nettles, D. L.; Setton, L. A.; Chilkoti, A. Rapid Cross-Linking of Elastin-like Polypeptides with (Hydroxymethyl)-phosphines in Aqueous Solution. *Biomacromolecules* **2007**, *8*, 1463−1470.
(27) Chung, C.; Lampe, K. J.; Heilshorn, S. C. Tetrakis-(hydroxymethyl) Phosphonium Chloride as a Covalent Cross-Linking Agent for Cell Encapsulation within Protein-Based Hydrogels. *Biomacromolecules* **2012**, *13*, 3912−3916.
(28) Wang, H.; Cai, L.; Paul, A.; Enejder, A.; Heilshorn, S. C. Hybrid Elastin-like Polypeptide-Polyethylene Glycol (ELP-PEG) Hydrogels with Improved Transparency and Independent Control of Matrix Mechanics and Cell Ligand Density. *Biomacromolecules* **2014**, *15*, 3421−3428.
(29) Xia, L.-W.; Xie, R.; Ju, X.-J.; Wang, W.; Chen, Q.; Chu, L.-Y. Nano-Structured Smart Hydrogels with Rapid Response and High Elasticity. *Nat. Commun.* **2013**, *4*, 2226.
(30) Wu, D.-Q.; Wu, J.; Chu, C.-C. A Novel Family of Biodegradable Hybrid Hydrogels from Arginine-Based Poly(ester Amide) and Hyaluronic Acid Precursors. *Soft Matter* **2013**, *9*, 3965.
(31) Ma, X.; Sun, X.; Hargrove, D.; Chen, J.; Song, D.; Dong, Q.; Lu, X.; Fan, T. H.; Fu, Y.; Lei, Y. A Biocompatible and Biodegradable Protein Hydrogel with Green and Red Autofluorescence: Preparation, Characterization and in Vivo Biodegradation Tracking and Modeling. *Sci. Rep.* **2016**, *6*, 1−12.
(32) Nordestgaard, B. G.; Rostgaard, J. Critical-Point Drying versus Freeze Drying for Scanning Electron Microscopy: A Quantitative and Qualitative Study on Isolated Hepatocytes. *J. Microsc.* **1985**, *137*, 189−207.
(33) Lenihouannen, D.; Guehennec, L.; Rouillon, T.; Pilet, P.; Bilban, M.; Layrolle, P.; Daculsi, G. Micro-Architecture of Calcium Phosphate Granules and Fibrin Glue Composites for Bone Tissue Engineering. *Biomaterials* **2006**, *27*, 2716−2722.
(34) Gusnard, D.; Kirschner, R. H. Cell and Organelle Shrinkage during Preparation for Scanning Electron Microscopy: Effects of Fixation, Dehydration and Critical Point Drying. *J. Microsc.* **1977**, *110*, 51−57.
(35) Weis-Fogh, T. A Rubber-like Protein in Insect Cuticle. *J. Exp. Biol.* **1960**, *37*, 889−907 http://jeb.biologists.org/content/37/4/889.article-info.
(36) Lloyd, D. J.; Garrod, M. A Contribution to the Theory of the Structure of Protein Fibres with Special Reference to the so-Called Thermal Shrinkage of the Collagen Fibre. *Trans. Faraday Soc.* **1948**, *44*, 441−451.
(37) Downes, A.; Mouras, R.; Elfick, A. A Versatile CARS Microscope for Biological Imaging. *J. Raman Spectrosc.* **2009**, *40*, 757−762.
(38) Lutolf, M. P.; Hubbell, J. A. Synthesis and Physicochemical Characterization of End-Linked Poly(ethylene Glycol)-Co-Peptide Hydrogels Formed by Michael-Type Addition. *Biomacromolecules* **2003**, *4*, 713−722.
(39) Kyburz, K. A.; Anseth, K. S. Three-Dimensional hMSC Motility within Peptide-Functionalized PEG-Based Hydrogels of Varying Adhesivity and Crosslinking Density. *Acta Biomater.* **2013**, *9*, 6381−6392.
(40) Chung, C.; Anderson, E.; Pera, R. R.; Pruitt, B. L.; Heilshorn, S. C. Hydrogel crosslinking density regulates temporal contractility of human embryonic stem cell-derived cardiomyocytes in 3D cultures. *Soft Matter* **2012**, *8*, 10141−10148.
(41) Bian, L.; Hou, C.; Tous, E.; Rai, R.; Mauck, R. L.; Burdick, J. A. The Influence of Hyaluronic Acid Hydrogel Crosslinking Density and Macromolecular Diffusivity on Human MSC Chondrogenesis and Hypertrophy. *Biomaterials* **2013**, *34*, 413−421.
(42) Wang, F.; Wang, Y.-C.; Dou, S.; Xiong, M.-H.; Sun, T.-M.; Wang, J. Doxorubicin-Tethered Responsive Gold Nanoparticles Facilitate Intracellular Drug Delivery for Overcoming Multidrug Resistance in Cancer Cells. *ACS Nano* **2011**, *5*, 3679−3692.
(43) Brown, S. D.; Nativo, P.; Smith, J.-A.; Stirling, D.; Edwards, P. R.; Venugopal, B.; Flint, D. J.; Plumb, J. A.; Graham, D.; Wheate, N. J. Gold Nanoparticles for the Improved Anticancer Drug Delivery of the Active Component of Oxaliplatin. *J. Am. Chem. Soc.* **2010**, *132*, 4678−4684.
(44) Ghosh, P.; Han, G.; De, M.; Kim, C.; Rotello, V. Gold nanoparticles in delivery applications☆. *Adv. Drug Deliv. Rev.* **2008**, *60*, 1307−1315.
(45) Rago, G.; Bauer, B.; Svedberg, F.; Gunnarsson, L.; Ericson, M. B.; Bonn, M.; Enejder, A. Uptake of Gold Nanoparticles in Healthy and Tumor Cells Visualized by Nonlinear Optical Microscopy. *J. Phys. Chem. B* **2011**, *115*, 5008−5016.
(46) Giljohann, D. A.; Seferos, D. S.; Daniel, W. L.; Massich, M. D.; Patel, P. C.; Mirkin, C. A. Gold Nanoparticles for Biology and Medicine. *Angew. Chem., Int. Ed.* **2010**, *49*, 3280−3294.
(47) Duncan, B.; Kim, C.; Rotello, V. M. Gold Nanoparticle Platforms as Drug and Biomacromolecule Delivery Systems. *J. Controlled Release* **2010**, *148*, 122−127.
(48) Fokong, S.; Theek, B.; Wu, Z.; Koczera, P.; Appold, L.; Jorge, S.; Resch-Genger, U.; van Zandvoort, M.; Storm, G.; Kiessling, F.; et al. Image-Guided, Targeted and Triggered Drug Delivery to Tumors Using Polymer-Based Microbubbles. *J. Controlled Release* **2012**, *163*, 75−81.
(49) Li, J.; Mooney, D. J. Designing Hydrogels for Controlled Drug Delivery. *Nat. Rev. Mater.* **2016**, *1*, 16071.
(50) Liu, J. C.; Tirrell, D. A. Cell Response to RGD Density in Cross-Linked Artificial Extracellular Matrix Protein Films. *Biomacromolecules* **2008**, *9*, 2984−2988.
(51) Straley, K. S.; Heilshorn, S. C. Independent Tuning of Multiple Biomaterial Properties Using Protein Engineering. *Soft Matter* **2009**, *5*, 114−124.
(52) Kimling, J.; Maier, M.; Okenve, B.; Kotaidis, V.; Ballot, H.; Plech, A. Turkevich Method for Gold Nanoparticle Synthesis Revisited. *J. Phys. Chem. B* **2006**, *110*, 15700−15707.
(53) Benitez, P. L.; Sweet, J. A.; Fink, H.; Chennazhi, K. P.; Nair, S. V.; Enejder, A.; Heilshorn, S. C. Sequence-Specific Crosslinking of Electrospun, Elastin-Like Protein Preserves Bioactivity and Native-Like Mechanics. *Adv. Healthcare Mater.* **2013**, *2*, 114−118.
(54) Enejder, A.; Brackmann, C.; Svedberg, F. Coherent Anti-Stokes Raman Scattering Microscopy of Cellular Lipid Storage. *IEEE J. Sel. Top. Quantum Electron.* **2010**, *16*, 506−515.

DOI: 10.1021/acsami.8b02461
ACS Appl. Mater. Interfaces 2018, 10, 21808−21815